CONFERENCE PRE-PRINT

ANOMALOUS X2-MODE ECRH POWER ABSORPTION AT THE TJ-II STELLARATOR: COMPARISON OF THEORY AND EXPERIMENTS

E.Z. GUSAKOV
Ioffe Institute
St.-Petersburg, Russia
Email: evgeniy.gusakov@mail.ioffe.ru

A.Y. POPOV
Ioffe Institute
St.-Petersburg, Russia
Email: a.popov@mail.ioffe.ru

Abstract

We propose a theoretical model interpreting the discrepancy between the launched and actually absorbed microwave power observed in X2 mode ECRH experiments at the TJ-II stellarator as a consequence of a parametric decay instability of the pump extraordinary wave and its saturation via a cascade of further decays, leading to the excitation of upper hybrid (UH) waves localized near a local maximum of the non-monotonic density profile, often measured in this device.

1. INTRODUCTION

The physics of burning plasma is getting closer to being demonstrated in ITER. This shifts the focus of fusion research in the current toroidal devices towards details and reliability testing of methods and techniques required for successful discharge control. The electron cyclotron resonance heating (ECRH) by powerful microwave beams is considered as an important method for localised plasma heating and current generation, which makes it possible to stabilize the neoclassical tearing mode (NTM) and to provide sawtooth control. Until recently, it was assumed that ECRH obeys predictions of linear wave propagation theory and that there are no pitfalls that would hinder the operation of this heating method. Spurious nonlinear phenomena, which can accompany the propagation of microwaves in inhomogeneous plasma and, in particular, parametric decay instabilities (PDIs), have been intensively studied since the early 1970s [1,2]. The results of the analysis were summarized in the review [3]. Based on the developed model [1,2], the stability limits for microwaves used for electron cyclotron resonance heating (ECRH) in toroidal fusion devices were investigated, and the extremely high threshold of the PDI excitation, ranging from tens of MW to GW for various decay scenarios, was predicted [4]. This made it possible both to assert that microwaves remain stable to any parametric decays in ECRH experiments operating with heating beams possessing a power of up to megawatt, and to believe in their locality and predictability. The latter made EC physics a highly valued technique.

However, recent experimental observations, namely anomalous microwave emission in a frequency range shifted up and down in respect to the gyrotron frequency by about the lower hybrid frequency [5-9] and plasma emission at half-integer harmonics of the pump wave frequency [7,9] prove the nonlinear behavior of sub-megawatt microwave beams. The physical phenomena reported in [5-9] have been observed when a microwave pump beam passed through a plasma region with a non-monotonic density profile. As predicted by the low-threshold PDI model [10], in this case the low-threshold excitation of the most dangerous absolute PDI is possible. The latter is manifested in the temporary growth of daughter waves, at least one of which is localized in the decay region due to the nonmonotonic density profile and finite width of the microwave beam. This model allows a detailed quantitative explanation of the anomalous phenomena observed in ECRH experiments at TEXTOR [11,12], ASDEX-Upgrade [13] and Wendelstein 7-X [14].

It should be noted that the X2-mode ECRH experiments have also shown a discrepancy between the launched and actually absorbed microwave power, as well as between the predicted and measured power deposition profiles, especially at a hollow density profile [15-17]. A possible explanation was given in [18], where it was shown that the low-threshold parametric decay of the pump wave in the local maximum of the density profile, often observed in X2-mode ECRH experiments, can lead to the appearance of a two-dimensionally localized upper hybrid (UH) wave and a daughter extraordinary wave running from the decay layer to the plasma edge. The primary instability is then saturated by a cascade of secondary decays into two-dimensionally localized UH and ion Bernstein (IB) waves. Depending on the number of steps in the cascade of secondary decays either moderate or strong anomalous absorption of pump power by the daughter waves was

predicted [10]. It seems rather obvious that in the case of strong anomalous absorption the daughter extraordinary wave, having gained a significant fraction of the pump power and propagating to the edge of the plasma, is absorbed far beyond the pump wave ECR layer. This can explain both the broadening of the pump power deposition and the lack of actually absorbed microwave power in the discharge core.

In this paper, using the theoretical approach described in [10, 18] we consider the results obtained in X2-mode ECRH experiments at the TJ-II stellarator and demonstrate strong density dependence of the pump wave absorption efficiency [17]. We compare experimental dependencies and the results of theoretical predictions.

2. CASCADE DECAY OF A PUMP EXTRAORDINARY WAVE LEADING TO THE EXCITATION OF LOCALIZED UPPER HYBRID WAVES

The parametric decay occurs in a small volume within which the decay resonance conditions for the numbers and frequencies of three waves are satisfied. This allows us to introduce the Cartesian coordinate system (x, y, z) with the x axis being along the flux coordinate and directed inwards, and the coordinates y and z being perpendicular to and align with the magnetic field on the magnetic surface. The local maximum of a non-monotonic UH frequency profile is supposed to coincide with the coordinate system origin. We consider a pump Gaussian beam of extraordinary (X) waves with frequency ω_0, width w and power P_0, propagating quasi-perpendicularly to the magnetic field. In the framework of the WKB approximation its electric field reads as follows

$$\mathbf{E}_0 = \mathbf{e}_X(\omega_0, x)\, a_0(x) \sqrt{\frac{2P_0}{n_x(\omega_0, x) c w^2}} \exp\left(-\frac{y^2}{2w^2} - \frac{z^2}{2w^2} + i\int^x k_x(\omega_0, x')dx' - i\omega_0 t \right) + c.c. \tag{1}$$

where a_0 is the dimensionless amplitude of the wave with the corresponding boundary condition $a_0\big|_{-\infty} = 1$;

$$\mathbf{e}_X(\omega) = -i\frac{g(\omega)}{\varepsilon(\omega)}\mathbf{e}_x + \mathbf{e}_y \tag{2}$$

is the polarization vector with $\mathbf{e}_x$ and $\mathbf{e}_y$ being the unit vectors in the corresponding directions, g and ε being the perpendicular components of the cold-plasma dielectric tensor; $n_x(\omega) = ck_x(\omega)/\omega$ is the refraction index along the direction of inhomogeneity;

$$k_x(\omega) = \frac{\omega}{c}\sqrt{\frac{\varepsilon(\omega)^2 - g(\omega)^2}{\varepsilon(\omega)}} \tag{3}$$

is the x - component of the wavenumber. Further, we analyze the pump wave decay into an extraordinary wave and an UH wave trapped in the vicinity of the local maximum of a nonmonotonic density profile. The electric field of the first daughter wave can be represented by means of the WKB approximation as follows

$$\mathbf{E}_s = \mathbf{e}_X^*(\omega_s, x)\, a_s(x) \sqrt{\frac{2T_e}{n_x(\omega_s, x) w^2}} \exp\left(i\int^x k_x(\omega_s, x')dx' + i\omega_s t \right) + c.c. \tag{4}$$

where a_s is the wave amplitude with the corresponding boundary condition $a_s\big|_{x\to\infty} = 1$. The potential of the second one has the following representation [10]

$$\varphi_{UH} = \sqrt{\frac{4T_e}{w^2 \omega_m D_{m\omega}}}\, a_m(y, z)\, \phi_m(x) \exp(-i\omega_m t) + c.c. \tag{5}$$

where $\omega_m = \omega_0 - \omega_s$, $a_m(y, z)$ is the dimensionless amplitude describing the potential distribution on a magnetic surface. According to [10], the eigenfunction ϕ_m describing the mode localized along the direction of the plasma inhomogeneity is represented as follows

$$\begin{gathered}\phi_m = \frac{1}{\sqrt{L_m^+(x)}} \exp\left(i\int_{x_l^*}^x q_x^+(\omega_m, \xi)d\xi - i\frac{\pi}{4} \right) + \frac{1}{\sqrt{L_m^-(x)}} \exp\left(i\int_{x_l^*}^x q_x^-(\omega_m, \xi)d\xi + i\frac{\pi}{4} \right), \\ L_m^{\pm}(x) = \left|D_q^{\pm}(x)\right| \int_{x_l^*}^{x_r^*} d\xi \left(\frac{1}{\left|D_q^+(\xi)\right|} + \frac{1}{\left|D_q^-(\xi)\right|} \right), \; D_q^{\pm} = \left| \frac{\partial D_{UH}}{\partial q_x} \right|_{q_x^{\pm}(x)}\end{gathered} \tag{6}$$

In equations (5) and (6) $q_x^{\pm}$ are two solutions of the local dispersion equation for a quasi-electrostatic wave with due account for a small electromagnetic correction, which is important near the resonance UH resonance, $D_{UH}\left(q_x^{\pm}\right)|_{\omega_m} = 0$ [19] derived at $q_z = 0$, the eigen frequency ω_m obeys the quantization condition

$$\int_{x_l^*}^{x_r^*} d\xi \left(q_x^+(\xi) - q_x^-(\xi) \right) = \pi(2m+1) \tag{7}$$

with $x_{l,r}^*$ being the coordinates of the turning points of the UH wave trapped in a potential well. In equation (5) we have also introduced the following notations

$$D_{m\omega} = \int_{x_l^*}^{x_r^*} \left(\frac{D_{m\omega}^+(\xi)}{L_m^+(\xi)} + \frac{D_{m\omega}^-(\xi)}{L_m^{+-}(\xi)} \right) d\xi \,, \; D_{m\omega}^{\pm} = \left| \frac{\partial D_{UH}}{\partial \omega} \right|_{q_{Ix}^{\pm}(\omega_m, x)} .$$

The primary instability is saturated as a result of the pump wave depletion and the subsequent decay of the primary localized UH wave. The secondary decay leads to the excitation the trapped UH wave (the UH mode possessing a number $n > m$) and an ion Bernstein (IB) wave running out the decay layer along the direction of plasma inhomogeneity. The secondary trapped UH wave is described in the same way as the primary one, i.e., by equation (5). The potential of the IB wave has the WKB representation as follows

$$\varphi_{IB} = \sqrt{\frac{4T_e}{w^2 \omega_I D_{I\omega}}} a_I(\mathbf{r}) \exp\left(i \int^x q_{Ix}(\xi) d\xi - i\omega_I t \right) + c.c. \tag{8}$$

where $\omega_I = \omega_m - \omega_n$; a_I is the amplitude of the IB wave; q_{Ix} is the solution of the local dispersion equation for an electrostatic wave $D_{IB}(q_{Ix})|_{\omega_I} = 0$ [19]; $D_{I\omega} = \left| \partial D_{IB} / \partial \omega \right|_{q_{Ix}, \omega_I}$.

At a nonmonotonic density profile, shown in Fig. 1, the localization region for the daughter UH wave, as well as the dispersion curve (see Fig.1), is asymmetric. Moreover, in this case the UH wave localization is possible only in the finite interval of its frequencies. This implies a finite number of localized eigenmodes in the plasma cavity. The cascade of subsequent decays continues as long as the excited daughter UH wave remains localized. Since the threshold of the decay into running daughter waves is much higher than the power of sub-megawatt microwave beams, the cascade of secondary decays in this case ceases.

Using the envelope function approximation [20], we can represent the amplitudes of all running daughter waves in terms of the amplitudes of the other two captured waves involved in the decay. For instance, in the case of the primary instability, the amplitude of the daughter extraordinary wave (4) is proportional to the product of the amplitudes of the pump wave (1) and the trapped UH wave (5) and represented as follows

$$a_s(\mathbf{r}) = \sqrt{\frac{P_0}{cw^2 B(x)^2}} \frac{a_m(y,z)}{\sqrt{\omega_m D_{m\omega}}} \exp\left(-\frac{y^2}{2w^2} - \frac{z^2}{2w^2} \right) \int_x^{\infty} dx' \frac{\chi_{pr}^{nl}(x') \phi_m(x')}{\sqrt{n_x(\omega_0, x') n_x(\omega_s, x')}} \exp\left(-i \int^{x'} \left(k_x(\omega_0, x'') + k_x(\omega_s, x'') \right) dx'' \right) \tag{9}$$

In the case of secondary, tertiary, and so on instabilities, the amplitudes of the daughter IB waves (8) are proportional to the product of the amplitudes of the two eigenmodes of the UH wave. The following is a representation of the amplitude of the secondary IB wave

$$a_I(\mathbf{r}) = -i \frac{a_m(y,z) a_n(y,z)}{\sqrt{\pi w^2}} \sqrt{\frac{4\pi e^2 \omega_I D_{I\omega}}{T_e \omega_m D_{m\omega} \omega_n D_{n\omega}}} \int_{-\infty}^{x} dx' \frac{\chi_{\sec}^{nl}(x')}{D_{Iq}(x')} \phi_m(x') \phi_n(x') \exp\left(-i \int^{x'} q_{Ix}(\omega_I, x') dx'' \right) \Bigg|_{\omega_I = \omega_m - \omega_n} \tag{10}$$

The amplitudes of subsequent IB waves are expressed in the same way. In equations (9) and (10) new notations are introduced. Namely, $B(x)$ is the magnetic field, $\chi_{pr}^{nl} = 4\pi\omega_s \left(\mathbf{e}_X(\omega_s, x) \cdot \boldsymbol{\sigma}^{nl}(\omega_s) \cdot \mathbf{e}_X^*(\omega_0, x) \right) / c^2$, $\boldsymbol{\sigma}^{nl}$ is the bilinear conductivity describing the coupling of the pump and primary extraordinary waves with the primary UH wave, $\chi_{\sec}^{nl}$ is the bilinear susceptibility describing the coupling of three electrostatic waves [10, 22]. Substituting (9) and (10) into equations describing all the steps of cascade decays and using the procedure of the perturbation theory [21], we finally arrive at the set of equations describing the amplitudes of all eigenmodes of the UH wave

$$\begin{cases} \dfrac{\partial a_m}{\partial t} - i\Lambda_{my} \dfrac{\partial^2 a_m}{\partial y^2} - i\Lambda_{mz} \dfrac{\partial^2 a_m}{\partial z^2} = \sqrt{\dfrac{\omega_m}{\omega_0}} \tilde{\gamma}_p a_m W\left(|a_m|^2 \right) - \sqrt{\dfrac{\omega_m}{\omega_n}} \tilde{\gamma}_s |a_n|^2 a_m \\ \dfrac{\partial a_n}{\partial t} + i\Lambda_{ny} \dfrac{\partial^2 a_n}{\partial y^2} + i\Lambda_{nz} \dfrac{\partial^2 a_n}{\partial z^2} = \sqrt{\dfrac{\omega_n}{\omega_m}} \tilde{\gamma}_s |a_m|^2 a_n - \sqrt{\dfrac{\omega_n}{\omega_r}} \tilde{\gamma}_t |a_r|^2 a_n \\ \dfrac{\partial a_r}{\partial t} - i\Lambda_{ry} \dfrac{\partial^2 a_r}{\partial y^2} - i\Lambda_{rz} \dfrac{\partial^2 a_r}{\partial z^2} = \sqrt{\dfrac{\omega_r}{\omega_n}} \tilde{\gamma}_t |a_n|^2 a_r - \ldots \\ \ldots \end{cases} \tag{11}$$

where

$$W = \int_{-\infty}^{\infty} \int_{\xi}^{\infty} \frac{d\xi d\xi'}{F(\lambda_p)} a_0(\xi) a_0^*(\xi') \exp\left(i\lambda_p (\xi - \xi') - i(\xi^3 - \xi'^3) \right), \; F(\lambda) = 2^{8/6} \int_0^{\infty} ds \exp\left(i\lambda \frac{s^2}{2^{1/3}} - is^6 - i\frac{\pi}{6} \right), \tag{12}$$

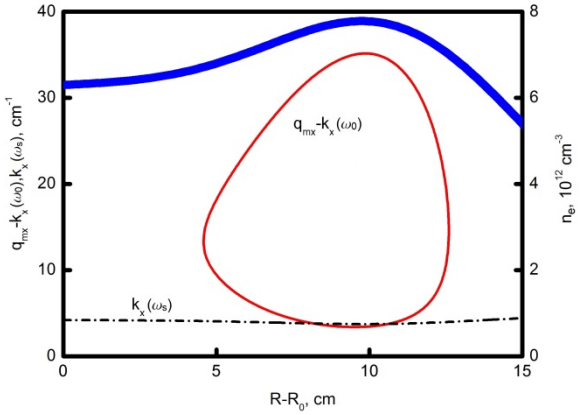

Figure 1. Dispersion curves illustrating primary instability. Right and bottom axes: the density profile n_e is depicted by the thick solid line [17]. Left and bottom axes: the 1D dispersion curve of the daughter UH wave (f_m=33.9 GHz, m = 38) down - shifted by the pump wave number (f_0 = 53.2 GHz) is shown by the thin solid line. The wave number of the daughter X1-mode is plotted by the dashed dotted line. The plasma parameters are as follows B_0=1 T, T_{e0} = 1 keV.

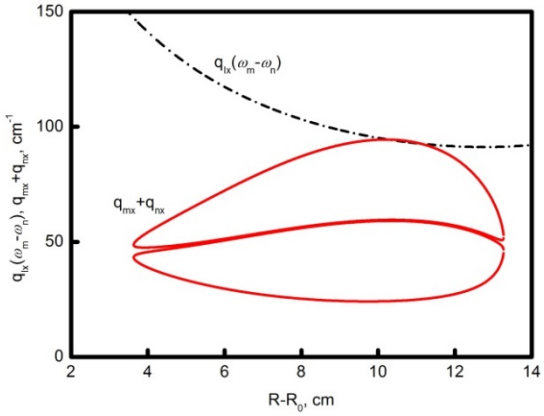

Figure 2. Dispersion curves illustrating secondary instability. The solid lines show the sum of the wavenumbers of two modes, m = 38 and n = 39, of the UH wave. The dashed dotted line shows the wavenumber of the IB wave with frequency f_I = 29.1 MHz.

$\lambda_p = \Delta K_p\left(x_{dp}\right) l_{dp}$, $l_{dp} = (|\, d^2\Delta K_p / dx^2\,|/6)^{-1/3}_{x_{dp}}$ is the length of the decay layer for the primary instability, x_{dp} is the coordinate of a point at which the mismatch for the decay resonance condition for the wavenumbers of the coupled waves $\Delta K_p = q^-_{mx} - k_{xs} - k_{x0}$ has its local minimum, and for a given $|a_m|^2$ the function a_0 is a numerical solution to the following ordinary differential equation describing the pump wave depletion:

$$\frac{\partial^2}{\partial\xi^2} a_0 - i\left(3\xi^2 - \lambda_p\right)\frac{\partial}{\partial\xi} a_0 - \gamma_p \frac{T_e}{P_0}\frac{\omega_0}{\omega_m}\left|a_m\left(y,z\right)\right|^2 a_0 = 0 \qquad (13)$$

Besides, $\tilde{\gamma}_j = \gamma_j F\left(\lambda_j\right)$, j = p,s,t, $\lambda_{s,t} = \Delta K_{s,t}\left(x_{ds,t}\right) l_{ds,t}$, x_{ds} and x_{dt} are the coordinates of two points where the mismatch of the decay resonance conditions for the wavenumbers of the coupled waves during the secondary $\Delta K_s = q^+_{mx} + q^+_{nx} - q_{Ix}$ and tertiary $\Delta K_t = q^+_{nx} + q^+_{rx} - q_{Ix}$ instabilities have their local minimum, *i.e.*, $d\Delta K_{s,t}\left(x_{ds,t}\right)/dx = 0$, $l_{ds,t} = |(d^2\Delta K_{s,t} / dx^2\,|/6)^{-1/3}_{x_{ds,t}}$ are the lengths of the decay layers for secondary and tertiary instabilities, γ_j, j = p,s,t are coefficients proportional to the plasma bilinear susceptibility [10, 22]. Depending on the number of excited eigenmodes of the UH wave, which is determined by the experimental conditions, the system of equations (11) should either be supplemented with additional equations or shortened.

In the forthcoming section, we will analyze the possibility of exciting low-threshold parametric decay instability of pump microwave for typical ECRH conditions in the X2 mode ECRH experiments at the TJ-II stellarator. We will compare the predictions of the theoretical model, which follow as a result of the numerical solution of the system of equations (11), with the experimental results and dependencies collected in X2-mode ECRH experiments at the TJ-II stellarator.

3. COMPARISON OF THEORETICAL PREDICTIONS AND THE TJ-II STELLARATOR EXPERIMENTAL RESULTS

The TJ-II stellarator is a heliac type device which has four periods for the magnetic field [23]. The average minor and major radii for the standard magnetic configuration are a = 0.22 m and R = 1.5 m. The toroidal magnetic field on the magnetic axis is B_0 = 1 T. The plasma heating is provided by launched microwave beams with a total power in the range of 200–500 kW. In the ECRH mode, the line average density is in the range of $\langle n_e \rangle$ = 0.3 - 1 × 10^{19} m^{-3}, and typical central electron and ion temperatures are correspondingly T_{e0} = 0.8–1.6 keV and T_{i0} = 80-120 eV.

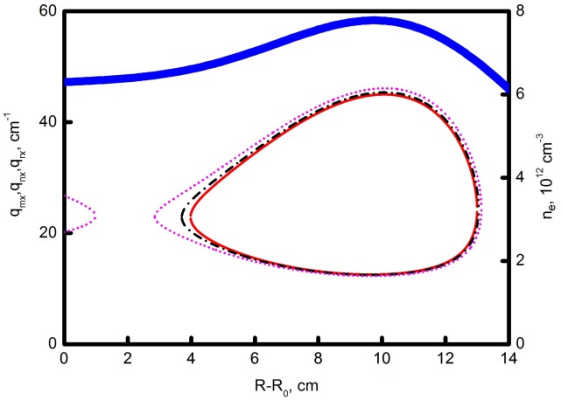

Figure 3. Dispersion curves of the modes (m = 38 - solid line; n = 39 - dashed line; r = 41 - dotted line) of the UH wave, which are excited at the density profile shown by the thick solid line.

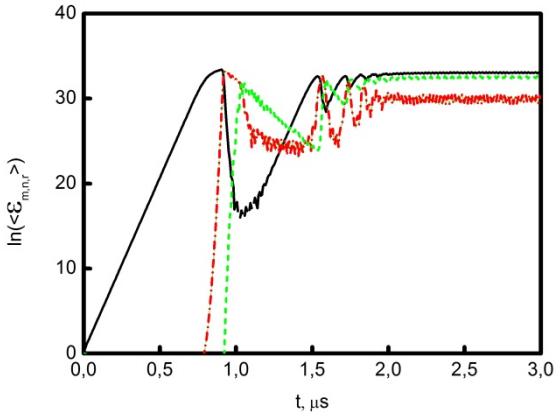

Figure 4. Temporal evolution of primary (solid curve), secondary (dashed-dotted curve) and tertiary (dashed curve) plasmons energies within the spot of a beam given in a semi-logarithmic scale. The same parameters as in figure 1, w = 2 cm and P_0 = 0.4 MW.

Figure 1 shows the dispersion curves illustrating the possibility of primary decay of the pump wave (1). A typical density profile n_e is depicted by the thick solid line [17]. It possesses an off-axis local maximum typical of an equilibrium magnetic configuration in TJ-II. The other parameters are taken as follows B_0 = 1 T, T_{e0} = 1.2 keV, T_{i0} = 90 eV. For this density profile the one-dimensional dispersion curve of the daughter UH wave q_x (f_m = 33.9 GHz, the mode number is equal to m=38) down - shifted by the pump wave number k_x (f_0 = 53.2 GHz) is shown by the thin solid line. The wave number k_{xs} of the daughter X1-mode is plotted by the dashed dotted line. In the region where dispersion curves are nearly tangent the decay resonance condition is fulfilled, i.e., $\Delta K_p = q_{mx} - k_x(\omega_0) - k_x(\omega_s) \approx 0$, and the PDI becomes possible. The daughter extraordinary wave being excited in the decay layer then propagates to the edge of the plasma. Figure 2 shows the dispersion curves illustrating secondary instability. The solid lines show the sum of the wavenumbers of two modes, m = 38 and n = 39, of the UH wave. The dashed dotted line shows the wavenumber of the IB wave with frequency f_I = 29.1 MHz. In the region where the dispersion curves touch, the decay resonance condition is fulfilled, i.e., $\Delta K_s = q_{mx} + q_{nx} - q_{Ix} \approx 0$, and secondary PDI of the primary UH wave occurs. The secondary UH wave (mode n) can further decay to the tertiary UH wave (mode r = 41). Figure 3 shows the dispersion curves of the modes (m = 38 - solid line, n = 39 - dashed line, r = 41 - dotted line) of the UH wave, which are excited at the density profile shown by the thick solid line and parameters used in figure 1. In the case under consideration the instability of the tertiary UH wave can only lead to the excitation of running UH and IB waves. The threshold of the latter phenomenon exceeds the tertiary wave amplitude, which interrupts the cascade of successive decays.

Then, we solve equations (11) and (13) numerically in a 2D box $2y_B \times 2z_B$. We assume the periodic boundary conditions with which the set of equations (11) and (13) describes non-physical multiple transitions of the daughter UH waves through the 2D box. Thereby, we can expect that the numerical solution obtained in this way remains meaningful at the time much less than the transition time of all the daughter waves through the 2D box. The results of numerical solution are shown in figure 4. The pump beam radius and the pump power were taken as w = 2 cm and P_0 = 0.4 MW. The figure shows the dimensionless energy densities of all primary, secondary and tertiary daughter waves, averaged over the spot of the pump beam according the mathematical procedure

$$<\varepsilon_j> = \int_S \frac{dydz}{\pi w^2} \left| a_j(y,z) \right|^2 \exp\left(-\frac{y^2}{w^2} - \frac{z^2}{w^2} \right), j = m,n,r, \qquad (14)$$

and given in semi-logarithmic scale. The exponential growth of the primary UH wave, i.e.., the excitation of absolute parametric decay instability, is shown by the solid line. The evolution of the secondary and tertiary waves is shown by the dashed dotted and dashed lines. The fast growth of them can be observed when the amplitude of the primary wave becomes large enough to overcome the threshold of their excitation. After some time, the instability goes into saturation mode. The primary and tertiary modes are saturated at a higher level than the secondary. In this case, the daughter waves acquire a significant fraction of the pump power [10].

Figure 5 shows the dependence of the anomalous absorption coefficient $\Delta P / P_0$ on the pump power P_0. In the considered case the threshold value is equal to $P_0^{th} = 204$ kW, which can be exceeded for microwave beams with a power of 200-500 kW typical of the X2-mode ECRH at the TJ-II stellarator [17].

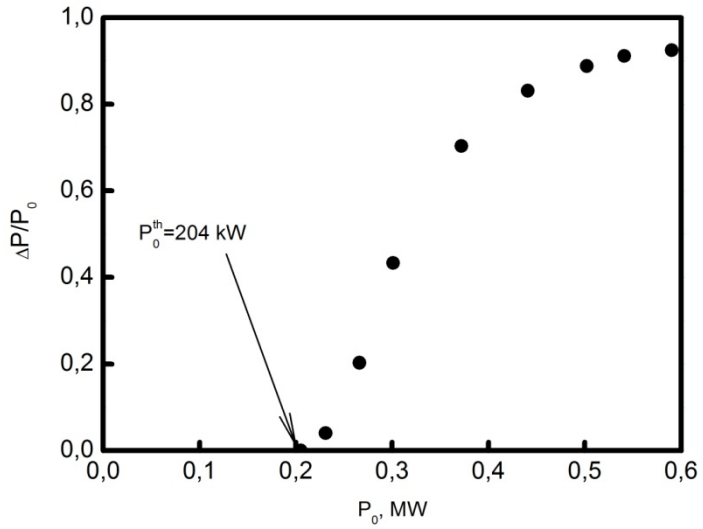

Figure 5. Dependence of the anomalous absorption coefficient on the pump power. The beam radius is w=2 cm.

Then, for the given radial profile (see figures 1, 3), we vary the central density and, by solving the system of equations (11) numerically, obtain different dependencies characterizing the instability. Figure 6 shows the dependence of the instability threshold on the average density. The parametric decay of the pump extraordinary wave (1) into the extraordinary wave (4) and the UH wave (5) can occur in a wide range of plasma densities that provide propagation conditions for both daughter waves. As the density increases, the trapped UH mode frequency increases, which leads to a decrease in the frequency of the X1-mode. The latter can propagate until the cut-off of a left-hand circularly polarized wave at

$$\omega_L = \frac{\sqrt{\omega_{ce}^2 + 4\omega_{pe}^2} - |\omega_{ce}|}{2} \quad . \tag{15}$$

Thus, the instability occurs when, for a given value of the magnetic field, the plasma density in the decay layer obeys the following inequality

$$\omega_0 - \sqrt{\omega_{ce}^2 + \omega_{pe}^2}\Big|_{x_{dp}} > \omega_L\big|_{x_{dp}} \tag{16}$$

When the latter condition is satisfied, both UH- and X1-modes of daughter waves exist. In the considered case inequality (9) is violated when the the chord averaged density exceeds the value $n_{cutoff} = 0.68 \times 10^{13}$ cm^{-3}. This makes the daughter extraordinary wave evanescent [24]. As a result, the excitation of primary instability becomes impossible, and the dependence shown in figure 6 is interrupted, i.e., the last point there corresponds to $<n_e> = 0.65 \times 10^{13}$ cm^{-3}.

The horizontal dashed line shows the typical power of a single microwave beam commonly used in X2-mode ECRH experiments at TJ-II [17]. It is seen that the higher the average density, the higher the instability threshold. When the average density exceeds the critical value of about $<n_e> = 0.6 \times 10^{13}$ cm^{-3}, the PDI excitation for a 330 kW beam becomes impossible. In this case, the absorption of the entire pump power occurs in the pump wave ECR layer as predicted by linear theory.

Figure 7 shows the dependence of the power fraction acquired by the daughter waves on the average density. In the low-density mode, there is a strong anomalous absorption of the pump power by the daughter waves whose ECR and collisional damping occurs far beyond the plasma core, which is expected to be the power deposition region during the on-axis X2-mode ECRH. The value $n^{(1)}$ is the transition boundary from a two-step cascade mode to a one-step cascade mode. The latter case corresponds to a weak anomalous absorption [10], as it is seen in figure 7. The value $n^{(2)}$ corresponds to the density at which the PDI threshold is equal to the pump power of 330 kW, and indicates the transition boundary from a mode when the pump wave is unstable to a mode with the stable pump wave. At densities greater than $n_{cutoff} = 0.68 \times 10^{13}$ cm^{-3}, the X1 mode becomes evanescent, and the decay is physically impossible. As it is seen in figure 7, at density values exceeding the value $n^{(2)}$, there is no anomalous absorption.

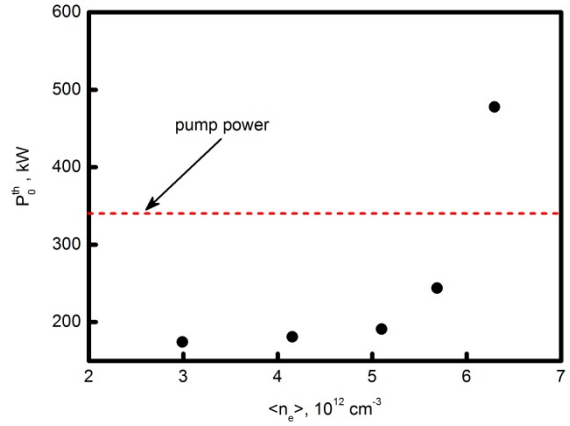

Figure 6. Dependence of the instability threshold on the value of the chord averaged density. The horizontal dashed line shows the typical power of a one microwave beam used in X2-mode ECRH experiments [17].

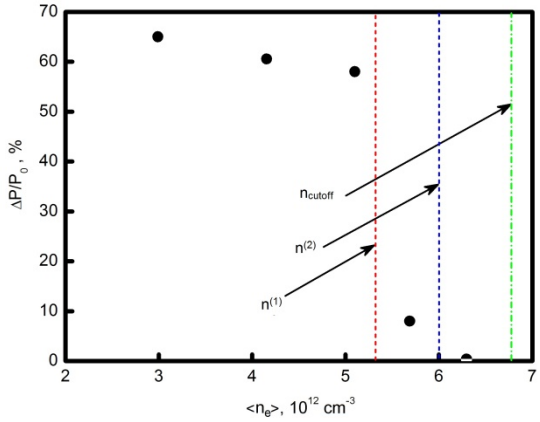

Figure 7. Dependence of the power fraction deposited to the daughter waves on the chord averaged density value. The value $n^{(1)}$ is the transition boundary from the mode with two-step decay cascade to the one-step cascade. The value $n^{(2)}$ indicates the density PDI threshold at the pump power of 330 kW. At densities greater than $n_{cutoff} = 0.68 \times 10^{13}\, cm^{-3}$, the X1 mode becomes evanescent, and the decay is physically impossible.

The considered decay scenario makes it possible to explain the dependence of the pump wave absorption efficiency on the average plasma density that was determined for TJ-II in [17]. In fact, the dependence shown in figure 7 is close to the dependence shown in figure 9, presented in [17]. The proposed model provides a possible explanation of the discrepancy between the launched and actually absorbed microwave power and its dependence on the average density, found in X2-mode ECRH experiments at TJ-II. It seems consistent and allows explaining the details of the experimental data collected in the TJ-II stellarator and analysed in [17]. To make a definite choice in favor of the proposed explanation direct observations of the extraordinary daughter wave at the plasma edge are needed.

4. CONCLUSIONS

In the paper we describe the theoretical model which allows interpreting the discrepancy between the launched and actually absorbed microwave power, observed in X2 mode ECRH experiments at the TJ-II stellarator, as a consequence of the pump extraordinary wave parametric decay instability and its saturation via a cascade of further decays, leading to the excitation of the running extraordinary wave and the upper hybrid waves localized near a local maximum of the non-monotonic density profile, often observed in this device [17]. The power acquired by daughter waves is absorbed far beyond the plasma core, which is expected to be a power deposition region during on-axis X2-mode ECRH at TJ-II [17]. In turn, the power of the pump wave remained after its decay and absorbed in the plasma core due to the ECR damping is less than the power launched into the plasma. The dependence of the power fraction deposited to the daughter waves on the chord averaged density value shown in figure 7 is close to the dependence of the missing power on density shown in figure 9, presented in [17].

5. ACKNOWLEDGEMENTS

The analytical treatment is supported under the RSF 22-12-00010-P grant, the numerical modelling – by the Ioffe Institute contract 0040-2024-0028 whereas the code for the PDI modelling was developed under the Ioffe Institute contract 0034-2021-0003.

6. REFERENCES

[1] ROSENBLUTH, M.N., Phys. Rev. Lett., **29** (1972) 565.
[2] PILIYA, A. D., JETP Letters, **17** (1973) 266.
[3] REIMAN, A., Reviews of Modern Physics, **51** (1979) 311.
[4] COHEN, B. I., COHEN, R. H., NEVINS, W. M., ROGNLIEN, T. D., Reviews of Modern Physics, **63** (1991) 949.
[5] WESTERHOF, E., NIELSEN, S. K., OOSTERBEEK, J. W., SALEWSKI, M., DE BAAR, M. R., BONGERS, W. A., BÜRGER, A., HENNEN, B. A., KORSHOLM, S. B., LEIPOLD, F., MOSEEV, D., STEJNER, M., THOEN, D.J., Phys. Rev. Lett., **103** (2009) 125001.
[6] NIELSEN, S. K., SALEWSKI, M., WESTERHOF, E., BONGERS, W., KORSHOLM, S. B., LEIPOLD, F., OOSTERBEEK, J. W., MOSEEV, D., STEJNER, M., Plasma Phys. Control. Fusion, **55** (2013)115003.
[7] HANSEN, S. K., NIELSEN, S. K., STOBER, J., RASMUSSEN, J., STEJNER, M., HOELZL, M., JENSEN, T., Nucl. Fusion, **60** (2020) 106008.
[8] TANCETTI, A., NIELSEN, S. K., RASMUSSEN, J., GUSAKOV, E. Z., POPOV, A. Y., MOSEEV, D., STANGE, T., SENSTIUS, M. G., KILLER, C., VECSEI, M., JENSEN, T., ZANINI, M., ABRAMOVIC, I., STEJNER, M., ANDA, G., DUNAI, D., ZOLETNIK , S., LAQUA, H., Nuclear Fusion, **62** (2022) 074003.
[9] CLOD, A., SENSTIUS, M. G., NIELSEN, A. H., RAGONA, R., THRYSØE, A. S., KUMAR, U., CODA, S., NIELSEN, S. K., Physical Review Letters, **132** (2024) 135101.
[10] GUSAKOV, E. Z., POPOV, A. Y., Phys. Usp., **63** (2020) 365.
[11] GUSAKOV, E. Z., POPOV, A. Y., Physics of Plasmas, **23** (2016) 082503.
[12] GUSAKOV, E. Z., POPOV, A. Y., Plasma Physics Reports, **49** (2023) 949.
[13] GUSAKOV, E. Z., POPOV, A. Y., TRETINNIKOV, P. V., Nucl. Fusion, **59** (2019) 106040.
[14] GUSAKOV, E. Z., POPOV, A. Y., Plasma Physics Reports, **49** (2023) 194.
[15] GUSAKOV, E. Z., POPOV, A. Y., MESHCHERYAKOV, A. I., GRISHINA, I. A., TERESHCHENKO, M. A., Phys. Plasmas, **30** (2023) 122112.
[16] EGUILIOR, S., CASTEJÓN, F., DE LA LUNA, E., CAPPA, A., LIKIN, K., FERNÁNDEZ, A., TJ-II TEAM, Plasma Phys. Control. Fusion, **45** (2003) 105.
[17] DNESTROVSKIJ, Y. N., MELNIKOV, A. V., LOPEZ-BRUNA, D., DNESTROVSKIJ, A. Y., CHERKASOV, S. V., DANILOV, A. V., ELISEEV, L. G., KHABANOV, F. O., LYSENKO, S. E., SYCHUGOV, D. Y., Plasma Phys. Control. Fusion, **65** (2023) 015011.
[18] POPOV, A. Y., GUSAKOV, E. Z., Phys. Plasmas, **31** (2024) 072104.
[19] SWANSON, D. G., Plasma waves - 2nd ed. - Bristol: IOP, (2003) 456 p.
[20] FEDORYUK, M. V., (1993) Asymptotic Analysis / Linear Ordinary Differential Equations Springer-Verlag Berlin Heidelberg.
[21] GUSAKOV, E. Z., FEDOROV, V. I. Sov. J. Plasma Phys., **5** (1979) 463.
[22] GUSAKOV, E. Z., POPOV, A. YU., TRETINNIKOV, P. V., Plasma Phys. Control. Fusion, **61** (2019) 085008.
[23] ALEJALDRE, C., GOZALO, J. J. A., PEREZ, J. B., MAGAÑA, F. C., DIAZ, J. R. C., PEREZ, J. G., LOPEZ-FRAGUAS, A., GARCÍA, L., KRIVENSKI, V., MARTÍN, R., NAVARRO, A. P., PEREA, A., RODRIGUEZ-YUNTA. A., AYZA, M. S., VARIAS, A., Fusion Sci. Technol., **17** (1990) 131.
[24] GUSAKOV, E. Z., POPOV, A. Y., Plasma Physics Reports, **49** (2023) 936.